Journal of Modern Optics

ISSN: 0950-0340 (Print) 1362-3044 (Online) Journal homepage: http://www.tandfonline.com/loi/tmop20

Comparison of different models employed to describe the z-scan curves for thick nonlinear optical media

Israel Severiano Carrillo , Marcela Maribel Méndez Otero , Maximino Luis Arroyo Carrasco & Marcelo David Iturbe Castillo

To cite this article: Israel Severiano Carrillo , Marcela Maribel Méndez Otero , Maximino Luis Arroyo Carrasco & Marcelo David Iturbe Castillo (2013) Comparison of different models employed to describe the z-scan curves for thick nonlinear optical media, Journal of Modern Optics, 60:3, 248-254, DOI: 10.1080/09500340.2013.769639

To link to this article: https://doi.org/10.1080/09500340.2013.769639

Journal of Modern Optics, 2013
Vol. 60, No. 3, 248–254, http://dx.doi.org/10.1080/09500340.2013.769639

Taylor & Francis
Taylor & Francis Group

Comparison of different models employed to describe the z-scan curves for thick nonlinear optical media

Israel Severiano Carrillo[a]*, Marcela Maribel Méndez Otero[a], Maximino Luis Arroyo Carrasco[a] and Marcelo David Iturbe Castillo[b]

[a]*Facultad de Ciencias Físico Matemáticas, Benemérita, Universidad Autónoma de Puebla, Puebla 72570, México;* [b]*Departamento de Óptica, Instituto Nacional de Astrofísica, Óptica y Electrónica, Tonantzintla 72840, México*

(*Received 17 December 2012; final version received 17 January 2013*)

A model that considers a photoinduced lens with a focal length dependent on a real power of the incident beam radius is compared with other reported models employed to describe the z-scan curves for thick media. It is demonstrated that this model is equivalent to that used to describe z-scan curves for thin nonlocal nonlinear media; then an extension is made for thick nonlocal nonlinear media. A comparison is made with other models to obtain z-scan curves for thick media. It is demonstrated that, under the same conditions, remarkable differences can be found in the simulated z-scan curves.

Keywords: z-scan; photoinduced focal length; nonlocal nonlinear media

1. Introduction

Characterization of the nonlinear optical properties of materials can be done using different methods. The z-scan technique is one of the most used due to its simplicity and accuracy. With this technique it is possible to obtain the sign and magnitude of the nonlinear refractive index, n_2, of a sample. The technique consists of displacing the sample along the optical axis (z-direction) of a focused laser beam, generally with Gaussian distribution, and detecting the transmitted power at the far field. This technique was first described theoretically and experimentally by Sheik-Bahae et al. [1]. A complete study of the main parameters that affect the technique was made by Chapple et al. [2]. Different modifications have been suggested in order to increase its sensitivity and its use with polarizing materials [3–9]. The z-scan technique is not restricted to implementation with Gaussian beams; other beam intensity distributions can be used [10–17].

There are different approaches to explain theoretically the technique for thin optical media. The first approach [1] was obtained using the Gaussian decomposition method [18], which is limited to samples with small phases. Samad et al. [19] used the Huygens–Fresnel principle to obtain an analytical expression of the on-axis far-field electric field and it was not limited to small phases. Since then, different approaches have been proposed and some of them employ of the aberration free approximation [20–24]. In [24], the nonlinear optical response of a thin media, under Gaussian illumination, was modeled as a photoinduced lens with a focal length dependent on the incident beam radius to a real power. Characteristics of the z-scan curves, such as peak–valley separation, peak–valley transmittance difference, and transmittance far from the focus, were found to be dependent on this power. The first model to describe the z-scan curves of thick media with Kerr nonlinearity was realized by Banerjee et al. [25]. Other models employing the aberration free approximation were reported in [26] and [27]. A model that considered the thermo-optical effect in the presence of linear and nonlinear absorption was presented in [28]. Zang et al. [29] proposed a model, using the Gaussian decomposition method and the distributed lens method, to analyze the z-scan technique for thick optical nonlinear media with nonlinear refraction and absorption. Pálfalvi et al. [30] presented a theory based on the solution of the nonlinear paraxial wave equation and the Huygens–Fresnel principle; this theory is valid for any sample thickness and large nonlinearities including both nonlinear refraction and absorption.

In this paper, we present an extension of the model of [24]. In the thin case, this model is compared with a nonlocal model to demonstrate their equivalence. The results obtained with this model are compared to those obtained with three other models used to describe the

*Corresponding author. Email: isevecar@hotmail.com

z-scan technique in thick media. Correspondences and differences are found for the different approaches. In the next section we describe the main results of the focal length model for thin media and its equivalence with a nonlocal model. In Section 3 we present the results obtained for thick media. In Section 4 we present a comparison of this model with the models reported by Magni et al. [26], Pálfalvi et al. [28] and Zang et al. [29], using the experimental parameters reported by Chapple et al. [31]. In Section 5 we present the conclusions of this work.

2. Thin media

The photoinduced focal length model was reported by Reynoso et al. [24] for thin media. There, the nonlinear response of the material, when it is illuminate by a Gaussian beam with beam waist ω_0, was considered as a photoinduced lens with a focal length F given by

$$F = a_r \omega^r \tag{1}$$

where a_r is a constant with the adequate units, that can include some parameters of the material, $\omega = \omega_0[1 + (z/z_0)^2]^{1/2}$ is the incident beam radius at the position z, z_0 is the Rayleigh distance given by $z_0 = \pi\omega_0{}^2/\lambda$, λ is the wavelength of the beam, and r is a real number that describes the type of nonlinearity of the material [24]. Under these considerations the far field normalized transmittance T was given by:

$$T = \frac{F^2}{z_0^2 + (F - z)^2}. \tag{2}$$

The main results obtained with this model, for small nonlinearity ($F > z_0$), were that the peak–valley position difference, Δz_{p-v}, given by

$$\Delta z_{p-v} = \frac{2}{\sqrt{r-1}}\, z_0 \tag{3}$$

and the peak–valley transmittance difference $\Delta T_{p\text{-}v}$, given by

$$\Delta T_{p-v} = \frac{2\Delta z_{p-v}}{F_{0r}}\left[\frac{(r-1)^r}{r^r}\right]^{1/2} \tag{4}$$

where $F_{0r} = a_r\omega_0{}^r$ depended on the value of r. Another important characteristic of the z-scan curves obtained with this model was that different values of r produced different behavior of the normalized transmittance with the position. This model was used to fit experimental results with good agreement. Two cases were considered, the first one with $r = 2$ for a dyed solution sample [32], and the second one with $r = 3$ for a dyed doped liquid crystal sample [33].

Recently, a model to describe the z-scan curves for thin nonlocal media was reported [34], where the peak valley position difference and the dependence of the normalized transmittance with position depended on the degree of nonlocality of the sample. Furthermore, the same set of experimental results (dyed solutions and liquid crystals) were fitted to the nonlocal model with good agreement. Thus, both models are equivalent and they can be used to describe nonlinear nonlocal media. This was demonstrated obtaining the z-scan curves under the same conditions but with different degrees of nonlocality [34] for only refractive nonlinearity. The z-scan curves obtained using Equation (1) presented a larger $\Delta T_{p\text{-}v}$ and smaller $\Delta z_{p\text{-}v}$ compared to those obtained in [34] for values of $r < 3.5$, whereas the differences were smaller for $r > 3.5$, as shown in Figure 1. The magnitude of a_r was adjusted to reproduce the behavior of samples with an on-axis phase shift, $\Delta\Phi_0$, equal to 0.1 rad and it was noted that both parameters are inversely related.

3. Z-scan for thick nonlocal media

To obtain the z-scan curves of thick samples with refractive nonlinearity illuminated with Gaussian beams we considered the thick sample as in the distributed-lens method [27]. The physical length of the sample L was divided in l units consisting of a thin lens, with a focal length of the type of Equation (1), and a linear media with refractive index n and length $d = L/l$. Knowing the beam waist of the incident Gaussian beam and using ABCD matrices for each unit, it is possible to calculate, numerically, the normalized transmittance of the z-scan technique. It is important to mention that in this case it is not possible to obtain an analytical formula for the normalized transmittance or a simple ABCD matrix for the thick media.

The behavior obtained for the z-scan curves with this model for different thickness samples is shown in Figures 2–4. In Figure 2, a photoinduced focal length lens with $r = 4$ and refractive index $n = 1.63$ was considered. The illuminating light was a Gaussian beam with $\omega_0 = 8.9$ μm at $\lambda = 532$ nm ($z_0 = 0.46$ mm). In Figures 3 and 4, we considered a photoinduced focal length lens with $r = 2$ and $r = 5$ and the rest of the parameters were equal to the ones used in Figure 2. For all the following calculations d was set equal to ω_0.

Figure 2 shows the z-scan curves for $r = 4$. The peak–valley position difference, $\Delta z_{p\text{-}v}$, increased as the thickness of the sample increased; the peak moved close to the origin and the valley away from it. The $z_{p\text{-}v}$ for thicknesses larger that $2z_0$ is approximately given by the length of the cell divided by n. The amplitude of the

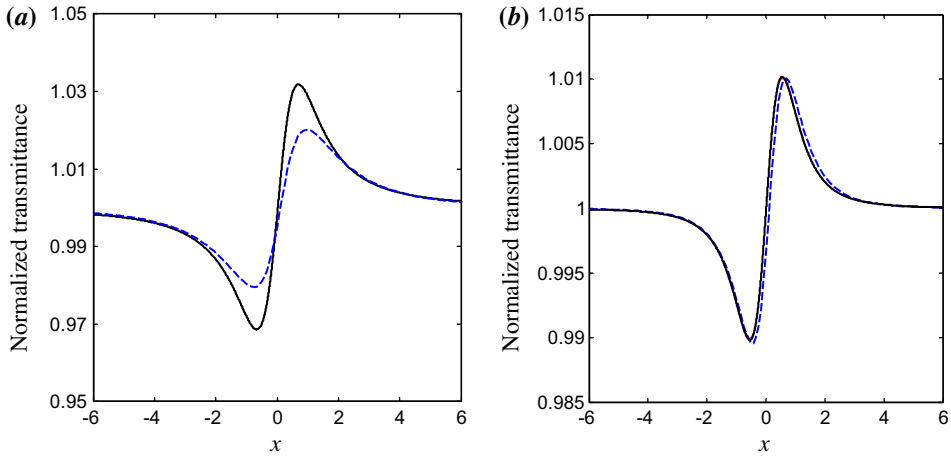

Figure 1. Z-scan curves using Equation (1) (solid line) with: (*a*) $r = 3.15$ and $a_r = 3 \times 10^9$ and (*b*) $r = 4.3$ and $a_r = 3.8 \times 10^{13}$ and z-scan curves using [34] (dashed line) with: (*a*) $m = 2$ and $\Delta\Phi_0 = 0.1$ rad and (*b*) $m = 4$ and $\Delta\Phi_0 = 0.1$ rad. For an incident Gaussian beam with $\omega_0 = 8.9$ μm and $\lambda = 532$ nm. (The color version of this figure is included in the online version of the journal.)

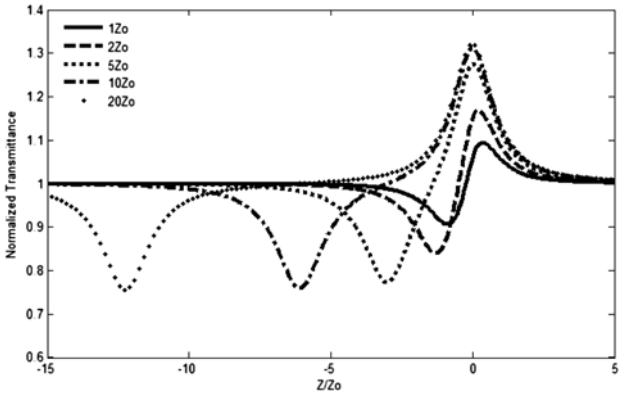

Figure 2. Numerical z-scan curves for a sample with $r = 4$ ($a_4 = 2.6 \times 10^{13}$) and $n = 1.63$, illuminated with a Gaussian beam of $\omega_0 = 8.9$ μm at $\lambda = 532$ nm and sample thickness of: z_0 (line), $2z_0$ (dashed line), $5z_0$ (dotted line), $10z_0$ (dashed-dot line), and $20z_0$ (point).

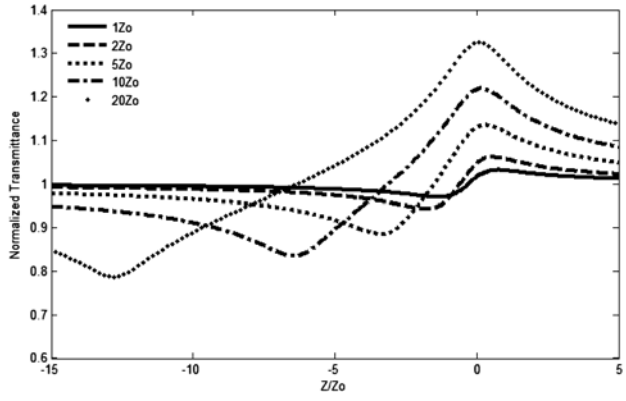

Figure 3. Numerical z-scan curves for a sample with $r = 2$ ($a_2 = 1 \times 10^8$) and sample thickness of: z_0 (line), $2z_0$ (dashed line), $5z_0$ (dotted line), $10z_0$ (dashed-dot line), and $20z_0$ (point). The other parameters are the same as for Figure 2.

peak increased for lengths of the sample smaller than $10z_0$, for thicker samples the amplitude of the peak did not change. A similar behavior was observed for the valley. The width of the peak (valley) was smaller than $1.5z_0$, giving rise to a region, between the peak and valley, with normalized transmittance close to one for the longest sample.

In Figure 3, the z-scan curves for $r = 2$ are presented. In general, a similar behavior to that obtained with $r = 4$ is observed; however, two main differences arise. The amplitude of the peak (valley) increased as the thickness of the sample increased. The width of the peak (valley) is larger than $4z_0$, and there is a region between the peak and the valley where the normalized transmittance changes linearly with position.

In Figure 4 we plot the z-scan curves obtained for $r = 5$. We can observe that they exhibit a similar behavior to the one obtained with $r = 4$. However, there are differences in the widths of the valley and the peak; they are thinner than those obtained in Figure 2. The amplitude of the peak increased for lengths of the sample smaller than $5z_0$, and for larger samples the amplitude of the peak did not change. A similar behavior was observed for the valley.

In Figure 5 we plot the peak–valley transmittance difference, $\Delta T_{p\text{-}v}$, as a function of the width of the sample for different values of r ($r = 2$ and $a_2 = 1 \times 10^8$, $r = 3$ and $a_3 = 4.2 \times 10^{10}$, $r = 4$ and $a_4 = 2.6 \times 10^{13}$, and $r = 5$ and $a_5 = 1.9 \times 10^{16}$). A refractive index of $n = 1.63$ was considered, the rest of the parameters were the same as the ones in the previous figures. It can be observed that as r increased, $\Delta T_{p\text{-}v}$ reached a constant

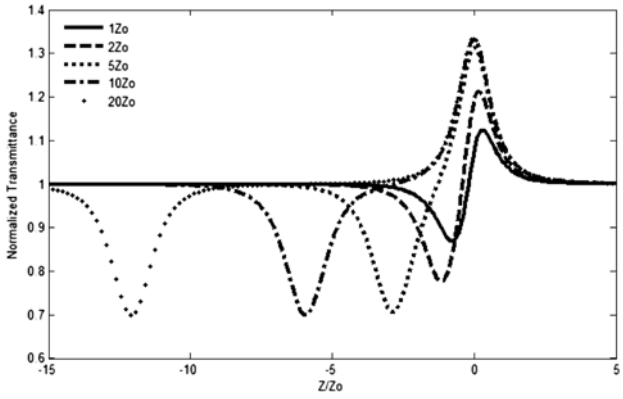

Figure 4. Numerical z-scan curves for a sample with $r = 5$ ($a_5 = 1.9 \times 10^{16}$) and sample thickness of: z_0 (line), $2z_0$ (dashed line), $5z_0$ (dotted line), $10z_0$ (dashed-dot line), and $20z_0$ (point). The other parameters are the same as for Figure 2.

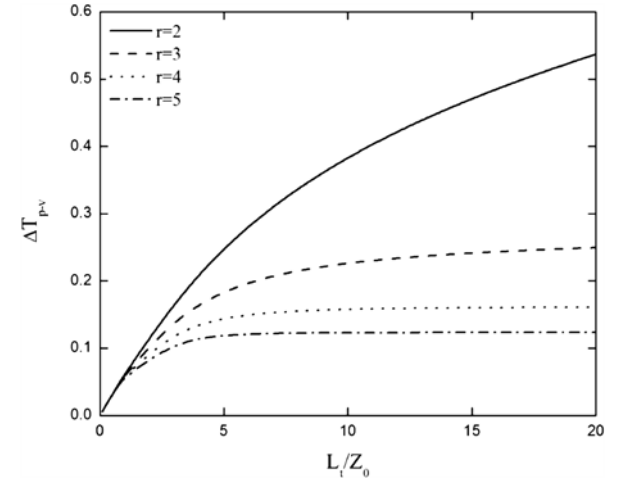

Figure 5. Numerical peak–valley transmittance difference as a function of the cell length (L_t) by different values for r. The other parameters are the same as for Figure 2.

value more rapidly. For thin samples, another point to note is that at the beginning all the curves have similar amplitudes, but as the length increased smaller values of r produced curves with larger amplitude.

In order to see the differences due to different values of r for the same cell length, in Figure 6 we plot the z-scan curves obtained for a cell length of $20z_0$ and values of $r = 2$, 3, 4, and 5. The rest of the parameters were the same as the ones employed in Figures 2 to 4. The magnitude of the constant used was chosen to give almost the same peak amplitude. As mentioned previously, the width of the peak increased as r decreased. The position of the peak is almost at $z/z_0 = 0$. However, the position of the valley depended on r. $\Delta z_{p\text{-}v}$ increased as r decreased. This behavior is very similar to the one obtained for a thin sample and different values of r [24].

Finally, it is important to mention that the same behavior is observed when the nonlinearity is negative

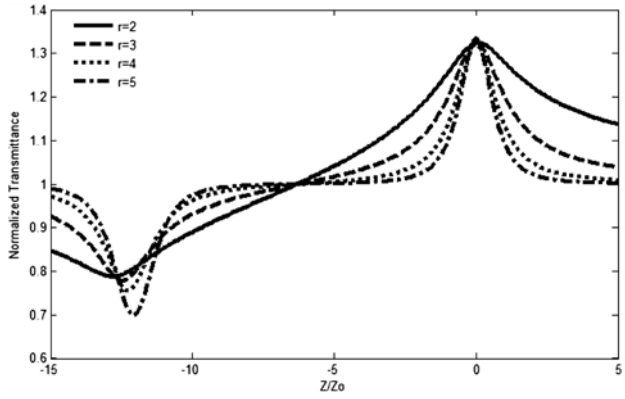

Figure 6. Numerical z-scan curves for a sample thickness of $20z_0$ for different r: $r = 2$ with $a_2 = 1 \times 10^8$ (line); $r = 3$, $a_3 = 4.2 \times 10^{10}$ (dashed line); $r = 4$, $a_4 = 2.6 \times 10^{13}$ (dotted line); and $r = 5$, $a_5 = 1.9 \times 10^{16}$ (dash-dot line). The other parameters are the same as for Figure 2.

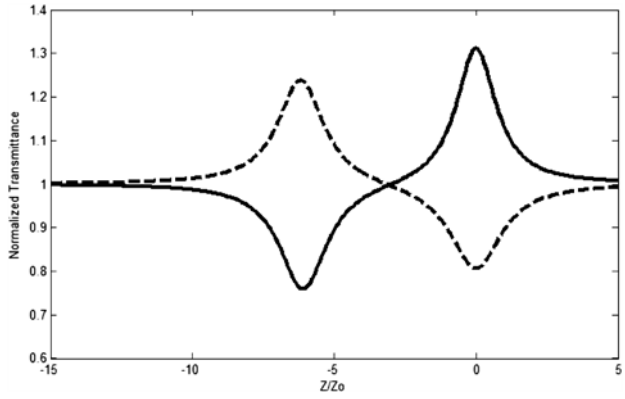

Figure 7. Numerical z-scan curves for a sample with $r = 4$ and $n = 1.63$, illuminated with a Gaussian beam of $\omega_0 = 8.9$ μm at $\lambda = 532$ nm and sample thickness of $10z_0$ with: $a_4 = 2.6 \times 10^{13}$ (line) and $a_4 = -2.6 \times 10^{13}$ (dashed line).

but with a difference in the amplitude of the curve, as is demonstrated in Figure 7, where two z-scan curves were obtained for the same constant magnitude, the same value of r, and the same cell thickness. It is observed that the curve for positive nonlinearity has a larger ΔT, whereas the position of the peak and valley for the two cases is practically the same.

The models proposed in other works for z-scan of thick media are for a local Kerr nonlinearity, the model presented here allows us to adjust different characteristics of the z-scan curve by changing the magnitude of r. In the next section we show how our model compares with some specific models.

4. Local models

In order to compare the results obtained with our model to the ones obtained with other models reported in the literature, in this section we described three different

approaches employed to describe the z-scan curves of thick media. The first model that we considered was that proposed by Magni et al. [26], the second by Pálfalvi et al. [28], and the third by Zang et al. [29].

4.1. Model 1

The model proposed by Magni et. al. [26] is based on the aberration free approximation, where the propagation of the Gaussian beam in the Kerr medium of length d is obtained with the following ABCD matrix:

$$M = \sqrt{1-\gamma}\begin{bmatrix} 1 & d_e \\ -\gamma/[(1-\gamma)d_e] & 1 \end{bmatrix}, \tag{5}$$

where $d_e = d/n_0$ is the effective length of the medium, n_0 is the refractive index of the medium and γ is defined as:

$$\gamma = \left[1 + \frac{1}{4}\left(\frac{2\pi\omega_c^2}{\lambda d_e} - \frac{\lambda d_e}{2\pi\omega_0}\right)^2\right]^{-1}\frac{P}{P_c} \tag{6}$$

where ω_c is the spot size at the center of the medium, ω_0 is the spot size at the beam waist, P is the incident power of the beam, and P_c is the critic power for self-focusing. This matrix is valid only for $\gamma < 1$. Note that when P/P_c tends to 0 the matrix reduces to the one for the propagation of a Gaussian beam in a homogeneous medium of refractive index n_0.

4.2. Model 2

The model proposed by Pálfalvi et al. [28] divides the thick medium in thin slices and compares each slice with a material with a gradient refractive index. The propagation of the incident Gaussian beam is obtained considered the following ABCD matrix:

$$M = \begin{bmatrix} \cos\left(\frac{lm}{l_{ef}/n_p}\right) & l_{ef}\cdot\sin\left(\frac{lm}{l_{ef}/n_p}\right) \\ -\frac{1}{l_{ef}}\cdot\sin\left(\frac{lm}{l_{ef}/n_p}\right) & \cos\left(\frac{lm}{l_{ef}/n_p}\right) \end{bmatrix}, \tag{7}$$

where lm is the thickness of nonlinear medium, n_p is the number of slices that the medium was divided and l_{ef} is the effective length defined as:

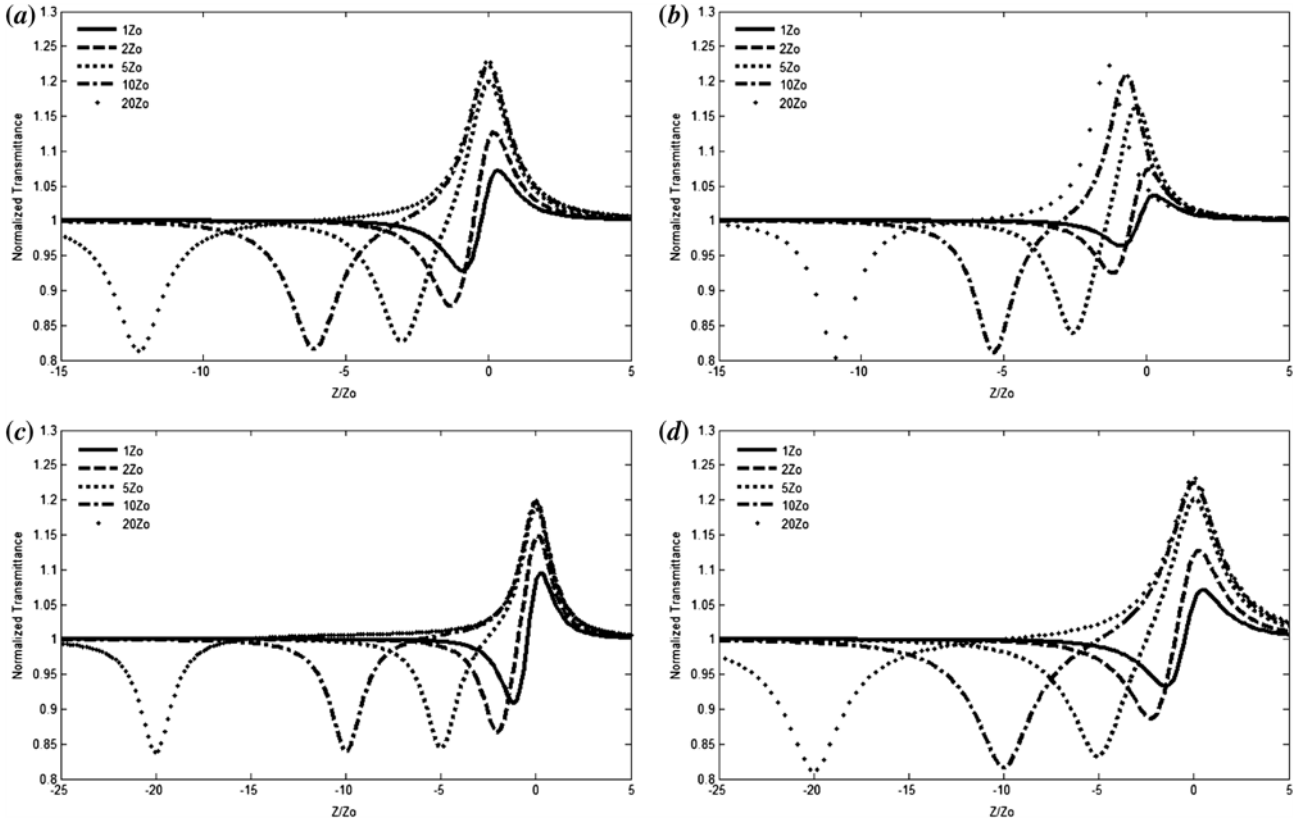

Figure 8. Numerical z-scan curves for the models for Kerr nonlinearity with $n = 1.63$ and illuminated with a Gaussian beam of $\omega_0 = 8.9$ μm at $\lambda = 532$ nm and sample thickness of: $1z_0$ (line), $2z_0$ (dashed line), $5z_0$ (dotted line), $10z_0$ (dashed-dot line), and $20z_0$ (point). (*a*) Model of focal length with $r = 4$ ($a_4 = 3.4 \times 10^{13}$); (*b*) model of Magni et al. [26] with $P = 0.24$; (*c*) model of Palfalvi et al. [28] with $n_2 = 2.7 \times 10^{-5}$; (*d*) model of Zang et al. [29] with $C_\phi(t) = 0.35$.

$$l_{ef}^2(z) = \frac{n_0\omega^4(z) + n_2 I_0 \omega_0^2 \omega^2(z)}{4 n_2 I_0 \omega_0^2} \tag{8}$$

where n_2 is the nonlinear refractive index of the media, I_0 is the on-axis intensity of the incident beam, and $\omega(z)$ is the beam radius at the position of the input face of the media.

4.3. Model 3

The last model that we consider is in fact a formula for the normalized transmittance of the z-scan technique proposed by Zang et al. [29]. They used the Gaussian decomposition method and a distributed lens model to obtain the following formula for the normalized transmittance T:

$$T = \left\{ \frac{[(x+l)^2+1] \times [(x^2+9)]}{[(x+l)^2+9] \times [(x^2+1)]} \right\}^{C_\varphi(t)/4}, \tag{9}$$

where:

$$C_\varphi(t) \cong \Delta\varphi_R(t) + \tanh(l/3) \times \left[[\Delta\varphi_R(t)]^2/4 + [\Delta\varphi_R(t)]^3/16 \right] \tag{10}$$

and $l = L/z_0$ is the length of medium, $x = z/z_0$ and $\Delta\phi_R(t) = k\Delta n_0(t) z_0$.

In Figure 8 we show the results obtained with our model and the ones obtained with the models proposed by Magni et al. [26], Pálfalvi et al. [28], and Zang et al. [29] for a medium with Kerr nonlinearity and sample thicknesses of $1z_0$, $2z_0$, $5z_0$, $10z_0$, and $20z_0$; the other parameters are the same as those employed in the previous section.

A comparison of the z-scan curves obtained with our model (Figure 8(*a*)) with those obtained with the model of Magni et al. [26] (Figure 8(*b*)) shows differences in the position and width of the peak and the valley; in our model the peak (valley) is wider than the one obtained from [26].

The position of the peak obtained in the z-scan curves for the models of [28] (Figure 8(*c*)) and [29] (Figure 8(*d*)) is very similar to the one obtained with our model (Figure 8(*a*)). However, the position of the valley was different. The width of the peak and the valley for the curves obtained with the model presented in [28] is smaller than the one obtained with the model of [29] and our model.

The peak and valley transmittance of the z-scan curves obtained with our model and that proposed in [26], [28], and [29], for sample lengths of $5z_0$, $10z_0$, and $20z_0$ was very similar for all models. Differences arose for sample lengths of $1z_0$ and $2z_0$ in all models. It is important to mention that the parameters selected for the calculation of the z-scan curves were the same as the ones used experimentally in [31]. We notice that our results reproduced with very good agreement the results reported in that paper.

5. Conclusions

In this paper we have demonstrated that a model that considers the nonlinear response of a thin nonlinear media as a lens with a focal length dependent on a real power r of the beam radius gives similar results to the ones obtained for nonlocal nonlinear media. This model was used to obtain z-scan curves of thick media for different nonlocalities, demonstrating that some characteristics of the curve depended on the r parameter. This model was compared with other models used to describe the z-scan technique for thick media, obtaining that the model we proposed, when the parameter r takes the value of 4, gives approximately the same behavior as the one obtained based on the Gaussian beam decomposition for a local media. This approach can be used to describe z-scan curves of thick samples that present a nonlocal nonlinear response where the physical origin of this behavior is unknown.

Acknowledgements

We gratefully acknowledge the support of the CONACYT.

References

[1] Sheik-Bahae, M.; Said, A.A.; Van Stryland, E.W. *Opt. Lett.* **1989,** *14,* 955–957.
[2] Chapple, P.B.; Staromlynska, J.; Hermann, J.A.; Mckay, T.J.; McDuff, R.G. *J. Nonlinear Opt. Phys. Mater.* **1997,** *6,* 251–293.
[3] Sheik-Bahae, M.; Wang, J.; DeSalvo, R.; Hagan, D.J.; Van Stryland, E.W. *Opt. Lett.* **1992,** *17,* 258–260.
[4] Xia, T.; Hagan, D.J.; Sheik-Bahae, M.; Van Stryland, E.W. *Opt. Lett.* **1994,** *19,* 317–319.
[5] Tian, J.-G.; Zang, W.-P.; Zhang, G. *Opt. Commun.* **1994,** *107,* 415–419.
[6] Marcano, O.; Maillotte, H.; Gindre, D.; Metin, D. *Opt. Lett.* **1996,** *21,* 101–103.
[7] Aguilar, P.A.; Mondragon, J.J.; Stepanov, S. *Opt. Lett.* **1996,** *21,* 1541–1543.
[8] Balu, M.; Hales, J.; Hagan, D.J.; Van Strayland, E.W. *Opt. Express.* **2004,** *12,* 3820–3826.
[9] Markowicz, P.; Samoc, M.; Cerne, J.; Prasad, P.N.; Pucci, A.; Ruggeri, G. *Opt. Express.* **2004,** *12,* 5209–5214.
[10] Bridges, R.E.; Fischer, G.L.; Boyd, R.W. *Opt. Lett.* **1995,** *20,* 1821–1823.
[11] Zhao, W.; Palffy-Muhoray, P. *Appl. Phys. Lett.* **1993,** *63,* 1613–1615.
[12] Rhee, B.K.; Byun, J.S.; Van Stryland, E.W. *J. Opt. Soc. Am. B* **1996,** *13,* 2720–2723.
[13] Zang, W.-P.; Tian, J.-G.; Liu, Z.-B.; Zhou, W.-Y.; Zhang, C.-P.; Zhang, G.-Y. *Appl. Opt.* **2003,** *42,* 2219–2225.

[14] Tsigaridas, G.; Fakis, M.; Polyzos, I.; Tsibouri, M.; Persephonis, P.; Giannetas, V.J. *Opt. Soc. Am. B* **2003,** *20,* 670–676.
[15] Huang, Y.-L.; Sun, C.-K.J. *Opt. Soc. Am. B* **2000,** *17,* 43–47.
[16] Gu, B.; Yan, J.; Wang, Q.; He, J.-L.; Wang, H.-T. *J. Opt. Soc. Am. B* **2004,** *21,* 968–972.
[17] Zang, W.-P.; Tian, J.-G.; Liu, Z.-B.; Zhou, W.-Y.; Song, F.; Zhang, C.-P. *Appl. Opt.* **2004,** *43,* 4408–4414.
[18] Weaire, D.; Wherrett, B.S.; Miller, D.A.B.; Smith, S.D. *Opt. Lett.* **1974,** *4,* 331–333.
[19] Samad, R.E.; Dias Vieira, N. *J. Opt. Soc. Am. B* **1998,** *15,* 2742–2747.
[20] Kwak, C.H.; Lee, Y.L.; Kim, S.G.J. *Opt. Soc. Am. B* **1999,** *16,* 600–604.
[21] Yao, B.; Ren, L.; Hou, X. *J. Opt. Soc. Am. B* **2003,** *20,* 1290–1294.
[22] Alves, S.; Bourdon, A.; Figueiredo Neto, A.M. *J. Opt. Soc. Am. B* **2003,** *20,* 713–718.
[23] Zang, W.-P.; Tian, J.-G.; Liu, Z.-B.; Zhou, W.-Y.; Song, F.; Zhang, C.-P.; Xu, J.-J. *J. Opt. Soc. Am. B* **2004,** *21,* 349–356.
[24] Reynoso Lara, E.; Navarrete Meza, Z.; Iturbe Castillo, M. D.; Treviño Palacios, C.G.; Martí Panameño, E.; Arroyo Carrasco, M.L. *Opt. Express* **2007,** *15,* 2517–2529.
[25] Banerjee, P.P.; Misra, R.M.; Maghraoui, M. *J. Opt. Soc. Am. B* **1991,** *8,* 1072–1080.
[26] Magni, V.; Cerullo, G.; De Silvestri, S. *Opt. Commun.* **1993,** *96,* 348–355.
[27] Sheik-Bahae, M.; Said, A.A.; Hagan, D.J.; Soileau, M.J.; Van Stryland, E.W. *Opt. Eng.* **1991,** *30,* 1228–1235.
[28] Pálfalvi, L.; Hebling, J. *Appl. Phys. B: Lasers Opt.* **2004,** *78,* 775–780.
[29] Zang, W.-P.; Tian, J.-G.; Liu, Z.-B.; Zhou, W.-Y.; Song, F.; Zhang, C.-P. *J. Opt. Soc. Am. B* **2004,** *21,* 63–66.
[30] Pálfalvi, L.; Tóth, B.C.; Almási, G.; Fülöp, J.A.; Hebling, J. *Appl. Phys. B: Lasers Opt.* **2009,** *97,* 679–685.
[31] Chapple, P.B.; Staromlynska, J.; McDuff, R.G.J. *Opt. Soc. Am. B* **1994,** *11,* 975–982.
[32] Iturbe Castillo, M.D.; Sánchez-Mondragón, J.J.; Stepanov, S.I. *Optik (Munich, Ger.)* **1995,** *100,* 49–56.
[33] Porras-Aguilar, R.; Ramirez-San-Juan, J.C.; Baldovino-Pantaleón, O.; May-Arrioja, D.; Arroyo Carrasco, M.L.; Iturbe Castillo, M.D.; Sánchez-de-la-Llave, D.; Ramos-Garcia, R. *Opt. Express* **2009,** *17,* 3417–3423.
[34] Garcia Ramirez, E.V.; Arroyo Carrasco, M.L.; Mendez Otero, M.M.; Reynoso Lara, E.; Chavez Cerda, S.; Iturbe Castillo, M.D. *J. Opt. (Bristol, U.K.)* **2011**, *13*, 085203.